Waves in Random and Complex Media
Vol. 18, No. 2, May 2008, 255–274

Taylor & Francis
Taylor & Francis Group

Scattering of electromagnetic waves from two-dimensional perfectly conducting random rough surfaces – study with the curvilinear coordinate method

Karim Aït Braham[a], Richard Dusséaux[a*] and Gérad Granet[b]

[a] *Université de Versailles Saint-Quentin en Yvelines, Centre d' étude des Environnements Terrestre et Planétaires (CETP), Vélizy, France;* [b] *Université Clermont-Ferrand II, Laboratoire des Sciences et Matériaux pour l'électronique et d'Automatique (LASMEA), Aubière, France*

(*Received 2 February 2007; final version received 12 October 2007*)

We present a method giving the bi-static scattering coefficient of two-dimensional (2-D) perfectly conducting random rough surface illuminated by a plane wave. The theory is based on Maxwell's equations written in a nonorthogonal coordinate system. This method leads to an eigenvalue system. The scattered field is expanded as a linear combination of eigensolutions satisfying the outgoing wave condition. The boundary conditions allow the scattering amplitudes to be determined. The Monte Carlo technique is applied and the bi-static scattering coefficient is estimated by averaging the scattering amplitudes over several realizations. The random surface is represented by a Gaussian stochastic process. Results are compared to published numerical and experimental data. Comparisons are conclusive.

1. Introduction

The problem of electromagnetic wave scattering from random surfaces continues to attract research interest because of its wide broad applications in optics, radio wave propagation and remote sensing. The analysis of rough surfaces with parameters close to the incident light wavelength requires a rigorous vectorial formalism. Numerous methods based on Monte Carlo simulations are available for the study of electromagnetic wave scattering from one-dimensional (1-D) and two-dimensional (2-D) random rough surfaces [1–4].

In previous papers, we have shown that the curvilinear coordinate method is an efficient and versatile theoretical tool for analysing 1-D rough surfaces [5–7]. The C method is based on Maxwell's equations written in a nonorthogonal coordinate system fitted to the structure geometry [5–10].

In the present paper, for the first time, the curvilinear coordinate method is applied for analysing 2-D perfectly conducting random rough surfaces. The scattering problem is presented in Section 2 and the C method is described in Section 3. Section 4 deals with the random scattering problem. The numerical procedure for the generation of a random surface is reported. The random surface is represented by a Gaussian stochastic process with a Gaussian roughness spectrum. The Monte Carlo technique is applied for estimating the averaged bi-static scattering coefficient and

*Corresponding author. Email: richard.dusseaux@cetp.ipsl.fr

ISSN: 1745-5030 print / 1745-5049 online

DOI: 10.1080/17455030701749328
http://www.informaworld.com

the incoherent intensity from the results over different realizations.The main aim of this paper is to present the principle of the C method applied to 2-D perfectly conducting random rough surfaces and to check our results by comparison with published numerical and experimental data (Section 5).

2. The field scattered from a rough surface

We consider a rough surface described by equation $z = a(x, y)$, where $a(x, y)$ is a local function defined over the surface area $L \times L$. The structure is illuminated by a monochromatic plane wave with wavelength λ. The incident wave vector $\vec{k}_i$ is defined by the zenith angle θ_i and the azimuth angle φ_i

$$\vec{k}_i = \alpha_i \vec{u}_x + \beta_i \vec{u}_y - \gamma_i \vec{u}_z \tag{1}$$

with

$$\alpha_i = k \sin\theta_i \cos\varphi_i; \quad \beta_i = k \sin\theta_i \sin\varphi_i; \quad \gamma_i = k \cos\theta_i \tag{2}$$

and

$$k = \frac{2\pi}{\lambda} \tag{3}$$

Both fundamental cases of horizontal and vertical polarizations are considered. For horizontal (or $E_{//}$) polarization, the electric field vector is parallel to the Oxy plane and for vertical (or $H_{//}$) polarization, this is the case for the magnetic field vector (4). The time-dependence factor varies as $\exp(j\omega t)$, where ω is the angular frequency. Hereafter, any vector function is represented by its associated complex vector function and the time factor is suppressed. Z is the intrinsic impedance of free space and the symbol $\wedge$ designates the vector product.

$$\left.\begin{matrix} \vec{E}_i^{(\mathrm{h})}(x, y, z) \\ Z\vec{H}_i^{(\mathrm{v})}(x, y, z) \end{matrix}\right\} = \vec{V}_i \exp(-j\vec{k}_i\vec{r}) \text{ and } Z\vec{H}_i = \frac{\vec{k}_i}{k} \wedge \vec{E}_i \tag{4}$$

with

$$\vec{V}_i = -\sin\varphi_i \vec{u}_x + \cos\varphi_i \vec{u}_y \tag{5}$$

and

$$\vec{r} = x\,\vec{u}_x + y\,\vec{u}_y + z\,\vec{u}_z \tag{6}$$

$\vec{u}_x$, $\vec{u}_y$ and $\vec{u}_z$ are the unit vectors of the Cartesian coordinate system (x, y, z).

Without any deformation, the total field is the sum of the incident field $(\vec{E}_i; \vec{H}_i)$ and the specularly reflected field $(\vec{E}_{sr}; \vec{H}_{sr})$ with

$$\left.\begin{matrix} \vec{E}_{sr}^{(\mathrm{h})}(x, y, z) \\ Z\vec{H}_{sr}^{(\mathrm{v})}(x, y, z) \end{matrix}\right\} = \rho\vec{V}_i \exp(-j\vec{k}_{sr}\vec{r}) \text{ and } Z\vec{H}_{sr} = \frac{\vec{k}_{sr}}{k} \wedge \vec{E}_{sr} \tag{7}$$

and

$$\vec{k}_{sr} = \alpha_i \vec{u}_x + \beta_i \vec{u}_y + \gamma_i \vec{u}_z \tag{8}$$

ρ is the Fresnel reflection coefficient with $\rho = -1$ and $\rho = 1$. For a locally deformed plane, we consider, in addition to the incident and reflected plane waves, a scattered field $\vec{E}_d^{(a)}(x, y, z)$. The problem consists in working out the h-polarized component and the v-polarized component:

$$\begin{aligned} \vec{E}_d^{(a)}(x, y, z) &= \vec{E}_d^{(aa)}(x, y, z) + \vec{E}_d^{(ba)}(x, y, z) \\ Z\vec{H}_d^{(a)}(x, y, z) &= Z\vec{H}_d^{(aa)}(x, y, z) + Z\vec{H}_d^{(ba)}(x, y, z) \end{aligned} \tag{9}$$

Hereafter, the upper script (a) denotes the incident plane wave polarization and (b), the scattered wave polarization.

Outside the modulated zone, the scattered field $\vec{E}_d^{(a)}(x, y, z)$ can be represented by a superposition of a continuous spectrum of outgoing plane waves [11, 12], the so-called Rayleigh integral. Above the highest point of the surface, the h-polarized component of scattered field is defined as follows

For $z > \max(a(x, y))$, $\forall x, y$,

$$\vec{E}_d^{(ha)}(x, y, z) = \frac{1}{4\pi^2} \int_{-\infty}^{+\infty} \int_{-\infty}^{+\infty} \hat{R}^{(ha)}(\alpha, \beta)\, \vec{V}(\alpha, \beta)\, \exp(-j\vec{k}_d(\alpha, \beta)\vec{r})\, d\alpha\, d\beta \tag{10}$$

$$\begin{aligned} Z\vec{H}_d^{(ha)}(x, y, z) = \frac{1}{4\pi^2} \int_{-\infty}^{+\infty} \int_{-\infty}^{+\infty} \hat{R}^{(ha)}(\alpha, \beta) \left(\frac{\vec{k}_d(\alpha, \beta)}{k} \wedge \vec{V}(\alpha, \beta) \right) \\ \times \exp(-j\vec{k}_d(\alpha, \beta)\vec{r})\, d\alpha\, d\beta \end{aligned} \tag{11}$$

with

$$\vec{k}_d(\alpha, \beta) = \alpha \vec{u}_x + \beta \vec{u}_y + \gamma \vec{u}_z; \quad Im(\gamma) \leq 0 \tag{12}$$

and

$$\vec{V}(\alpha, \beta) = -\frac{\beta}{\sqrt{\alpha^2 + \beta^2}} \vec{u}_x + \frac{\alpha}{\sqrt{\alpha^2 + \beta^2}} \vec{u}_y \tag{13}$$

When $\alpha^2 + \beta^2 > k^2$, $\gamma(\alpha, \beta)$ is a pure imaginary and the corresponding waves are evanescent waves. Otherwise, γ is real and the propagation vector $\vec{k}_d$ of the propagating wave is defined by the zenith angle θ and the azimuth angle φ.

$$\begin{cases} \alpha = k \sin\theta \cos\varphi \\ \beta = k \sin\theta \sin\varphi \\ \gamma\,(\alpha, \beta) = \sqrt{k^2 - \alpha^2 - \beta^2} = k \cos\theta \end{cases} \tag{14}$$

In the far-field zone, the Rayleigh expansion (10–11) is reduced to the only contribution of the propagating waves. The method of stationary phase leads to the asymptotic field [13, 14] at the point $M(r, \theta, \varphi)$:

$$\vec{E}^{(\mathrm{ha})}_{dfar}(r,\theta,\varphi) = -\hat{R}^{(\mathrm{ha})}(k\sin\theta\cos\varphi\,;\,k\sin\theta\sin\varphi) \cos\theta\frac{\exp(-jkr)}{\lambda r}\exp\left(-j\frac{\pi}{2}\right)\vec{u}_{\varphi} \tag{15}$$

$$Z\vec{H}^{(\mathrm{ha})}_{dfar}(r,\theta,\varphi) = \hat{R}^{(\mathrm{ha})}(k\sin\theta\cos\varphi\,;\,k\sin\theta\sin\varphi) \cos\theta\frac{\exp(-jkr)}{\lambda r}\exp\left(-j\frac{\pi}{2}\right)\vec{u}_{\theta} \tag{16}$$

Substituting $\vec{E}^{(\mathrm{ha})}$ by $Z\vec{H}^{(\mathrm{va})}$ and $Z\vec{H}^{(\mathrm{ha})}$ by $-\vec{E}^{(\mathrm{va})}$ in Equations (10), (11), (15) and (16) we obtain the v-polarized components of magnetic and electric field vectors. For an incident wave in (a) polarization and a scattered wave in (b) polarization, the normalized bistatic scattering coefficient $\sigma^{(\mathrm{ba})}(\theta,\varphi)$ is defined as follows

$$\sigma^{(\mathrm{ba})}(\theta,\varphi) = \frac{1}{P_i^{(\mathrm{a})}}\frac{dP_s^{(\mathrm{ba})}}{d\Omega} = \frac{\left|\hat{R}^{(\mathrm{ba})}(k\sin\theta\cos\varphi\,;\,k\sin\theta\sin\varphi)\,\cos\theta\right|^2}{\lambda^2 L^2\cos\theta_i} \tag{17}$$

$\frac{dP_s^{(\mathrm{ba})}}{d\Omega}$ is the power scattered per unit solid angle $d\Omega = \sin\theta\,d\theta\,d\varphi$ with

$$dP_s^{(\mathrm{ba})} = \frac{1}{2}\mathrm{Re}\left[\left(\vec{E}^{(\mathrm{ba})}_{dfar}\wedge\vec{H}^{(\mathrm{ba})*}_{dfar}\right)dS\vec{u}_r\right] \tag{18}$$

The symbol * designates the complex conjugate. dS is the element surface with $dS = r^2 d\Omega$. The unit vectors $\vec{u}_r$, $\vec{u}_\theta$ and $\vec{u}_\varphi$ are drawn in the direction of increasing r, θ and φ such as to constitute a right-hand base system. $P_i^{(\mathrm{a})}$ is the flux of incident power through the modulated region:

$$P_i^{(\mathrm{a})} = \frac{1}{2}\int_{-L/2}^{+L/2}\int_{-L/2}^{+L/2}\mathrm{Re}\left[\left(\vec{E}_i^{(\mathrm{a})}\wedge\vec{H}_i^{(\mathrm{a})*}\right)dxdy\vec{u}_z\right] \tag{19}$$

The normalised bi-static scattering coefficients fulfil the power balance criterion (20) [6, 14, 15].

$$P_s^{(a)} = P_{si}^{(a)} \tag{20}$$

with

$$P_s^{(a)} = \int_{\theta=-\pi/2}^{\theta=+\pi/2}\int_{\varphi=0}^{\varphi=\pi}(\sigma^{(\mathrm{aa})}(\theta,\varphi)+\sigma^{(\mathrm{ba})}(\theta,\varphi))\,d\theta d\varphi \tag{21}$$

$$P_{si}^{(a)} = -\frac{2\rho^{(\mathrm{a})}}{L^2}\mathrm{Re}\left(\hat{R}^{(\mathrm{aa})}(k\sin\theta_i\cos\varphi_i\;;\;k\sin\theta_i\sin\varphi_i)\right) \tag{22}$$

$P_s^{(a)}$ is the ratio between the total scattered power and the incident power in the polarization (a). $P_{si}^{(a)}$ represents the electromagnetic coupling between the incident, reflected and scattered waves divided by the incident power [14]. In subsection 5.2, the method is numerically investigated in the far-field zone by means of convergence on the power balance criterion.

3. Analysis with the curvilinear coordinate method

3.1. *Coordinate system – covariant components of field*

The scattered field cannot be expressed by the Rayleigh integral in the modulated zone if the perturbation amplitude is too large [11]. We can obtain an expression of fields that is valid over the surface by solving Maxwell's equations in the translation coordinate system. This system is obtained from the Cartesian system (x, y, z) [8, 10]

$$\begin{cases} x' = x \\ y' = y \\ z' = z - a(x, y) \end{cases} \tag{23}$$

In this new coordinate system, the height function $z = a(x, y)$ coincides with the coordinate surface $z' = 0$ [8] and the change from Cartesian components $(K_x;\ K_y;\ K_z)$ of vector $\vec{K}$ to covariant components $(K_{x'};\ K_{y'};\ K_{z'})$ is given by [8, 10, 16]

$$\begin{cases} K_{x'}(x';\ y';\ z') = K_x(x;\ y;\ z) + \dfrac{\partial a(x,\ y)}{\partial x} K_z(x;\ y;\ z) \\ K_{y'}(x';\ y';\ z') = K_y(x;\ y;\ z) + \dfrac{\partial a(x,\ y)}{\partial y} K_z(x;\ y;\ z) \\ K_{z'}(x';\ y';\ z') = K_z(x;\ y;\ z) \end{cases} \tag{24}$$

The covariant component $K_{z'}$ is simply the vertical component K_z. Moreover, the covariant components $K_{x'}$ and $K_{y'}$ are parallel to surface coordinate $z' = z_0$ and in particular, parallel to interface $z' = 0$.

In a source-free medium, it can be shown from the time harmonic Maxwell equations and the constitutive relations expressed in the translation system that the longitudinal components $E_{z'}$ and $ZH_{z'}$ obey to the same propagation Equation (25) [10]

$$\begin{aligned} &-\frac{\partial}{\partial z'}\left[g^{x'z'}\frac{\partial \psi}{\partial x'} + \frac{\partial\, g^{x'z'}\psi}{\partial x'}\right] - \frac{\partial}{\partial z'}\left[g^{y'z'}\frac{\partial \psi}{\partial y'} + \frac{\partial\, g^{y'z'}\psi}{\partial y'}\right] + jkg^{z'z'}\frac{\partial \psi'}{\partial z'} \\ &= \frac{\partial^2 \psi}{\partial x'^2} + \frac{\partial^2 \psi}{\partial y'^2} + k^2\psi \end{aligned} \tag{25}$$

with

$$\psi' = \frac{j}{k}\frac{\partial \psi}{\partial z'} \tag{26}$$

and $\psi(x', y', z') = E_{z'}(x', y', z')$ or $ZH_{z'}(x', y', z')$. $g^{x'z'}$, $g^{y'z'}$ and $g^{z'z'}$ are elements of metric tensor which depend on the derivatives of function $a(x', y')$ with respect to x' and y' [10]

$$\begin{aligned} g^{x'z'} &= -\frac{\partial a}{\partial x'} \\ g^{y'z'} &= -\frac{\partial a}{\partial y'} \\ g^{z'z'} &= 1 + \left(\frac{\partial a}{\partial x'}\right)^2 + \left(\frac{\partial a}{\partial y'}\right)^2 \end{aligned} \tag{27}$$

We obtain expressions of components E'_x, E'_y, H'_x and H'_y in terms of longitudinal components $E_{z'}$ and $ZH_{z'}$ only [10]

$$\frac{\partial^2 E_{x'}}{\partial z'^2} + k^2 E_{x'} = \frac{\partial^2 E_{z'}}{\partial x' \partial z'} - k^2 g^{x'z'} E_{z'} - jk g^{y'z'} \frac{\partial ZH_{z'}}{\partial z'} - jk \frac{\partial ZH_{z'}}{\partial y'} \tag{28}$$

$$\frac{\partial^2 E_{y'}}{\partial z'^2} + k^2 E_{y'} = \frac{\partial^2 E_{z'}}{\partial y' \partial z'} - k^2 g^{y'z'} E_{z'} + jk g^{x'z'} \frac{\partial ZH_{z'}}{\partial z'} + jk \frac{\partial ZH_{z'}}{\partial x'} \tag{29}$$

$$\frac{\partial^2 ZH_{x'}}{\partial z'^2} + k^2 ZH_{x'} = \frac{\partial^2 ZH_{z'}}{\partial x' \partial z'} - k^2 g^{x'z'} ZH_{z'} + jk g^{y'z'} \frac{\partial E_{z'}}{\partial z'} + jk \frac{\partial E_{z'}}{\partial y'} \tag{30}$$

$$\frac{\partial^2 ZH_{y'}}{\partial z'^2} + k^2 ZH_{y'} = \frac{\partial^2 ZH_{z'}}{\partial y' \partial z'} - k^2 g^{y'z'} ZH_{z'} - jk g^{x'z'} \frac{\partial E_{z'}}{\partial z'} - jk \frac{\partial E_{z'}}{\partial x'} \tag{31}$$

The covariant components $E_{x'}$ and $E_{y'}$ are parallel to the perfectly conducting interface. Consequently, we have $E_{x'} = E_{y'} = 0$ at $z' = 0$ (i.e. $z = a(x, y)$). In the next subsection, we propose a procedure for solving the propagation Equation (25)-(26) in the spectral domain [7]. The Oz-components are expanded as a linear combination of eigensolutions satisfying the outgoing wave condition. We deduce from Equations (28) to (31) the h-polarised components of electric and magnetic fields $\vec{E}_d^{(\mathrm{ha})}$ and $\vec{H}_d^{(\mathrm{ha})}$ by taking $E_{z'} = 0$ and the v-polarized components $\vec{E}_d^{(\mathrm{va})}$ and $\vec{H}_d^{(\mathrm{va})}$ by taking $H_{z'} = 0$. Finally, both h-polarized and v-polarized amplitudes of eigensolutions are found by solving the boundary conditions.

3.2. *Eigenvalues system and elementary wave functions*

After a Fourier transform (TF) with respect to x' and y', Equations (25) and (26) take the following form

$$\begin{aligned} &\frac{\partial}{\partial z'}\left[j\alpha(\hat{g}^{x'z'} * \hat{\psi}) + j\hat{g}^{x'z'} * (\alpha\,\hat{\psi}) + j\beta(\hat{g}^{y'z'} * \hat{\psi}) + j\hat{g}^{y'z'} * (\beta\,\hat{\psi})\right] \\ &+ jk\,\hat{g}^{z'z'} * \frac{\partial \hat{\psi}'}{\partial z'} = \gamma^2 \hat{\psi} \end{aligned} \tag{32}$$

$$\frac{j}{k}\frac{\partial \hat{\psi}}{\partial z'} = \hat{\psi}' \tag{33}$$

$\hat{K} * \hat{L}$ is the convolution product of two Fourier Transforms $\hat{K}(\alpha, \beta, z')$ and $\hat{L}(\alpha, \beta)$. In a second stage, convolution products are approximated as follows

$$(\hat{K} * \hat{L})(\alpha, \beta, z') = \frac{1}{4\pi^2} \int_{-\infty}^{+\infty} \int_{-\infty}^{+\infty} \hat{K}(\alpha', \beta', z')\, \hat{L}(\alpha - \alpha', \beta - \beta')\, d\alpha'\, d\beta'$$
$$\approx \frac{\Delta\alpha^2}{4\pi^2} \sum_p \sum_q \hat{K}(\alpha_p, \beta_q, z')\, \hat{L}(\alpha - \alpha_p, \beta - \beta_q) \tag{34}$$

where

$$\alpha_p = k \sin\theta_i \cos\varphi_i + p\Delta\alpha, \quad \beta_q = k \sin\theta_i \sin\varphi_i + q\Delta\alpha \tag{35}$$

$\Delta\alpha$ is the spectral resolution. As $\Delta\alpha$ decreases, approximations (34) become more accurate. Finally, from substituting Equation (34) into Equations (32) to (33) and applying the point matching method at discrete values $(\alpha_s; \beta_t)$, we obtain two sets of coupled first-order differential equations relating coefficients $\hat{\psi}(\alpha_s, \beta_t, z')$ and $\hat{\psi}'(\alpha_s, \beta_t, z')$ to each other.

$$\frac{j}{k} \frac{\partial}{\partial z'} \left(\sum_{p,q} \left(\frac{\alpha_s}{k} \hat{g}^{x'z'}_{s-p,t-q} + \hat{g}^{x'z'}_{s-p,t-q} \frac{\alpha_p}{k} + \frac{\beta_t}{k} \hat{g}^{y'z'}_{s-p,t-q} + \hat{g}^{y'z'}_{s-p,t-q} \frac{\beta_q}{k} \right) \hat{\psi}(\alpha_p, \beta_q, z') \right)$$
$$+ \frac{j}{k} \frac{\partial}{\partial z'} \left(\sum_{p,q} \hat{g}^{z'z'}_{s-p,t-q}\, \hat{\psi}'(\alpha_p, \beta_q, z') \right) = \frac{\gamma_{st}^2}{k^2} \hat{\psi}(\alpha_s, \beta_t, z') \tag{36}$$

$$\frac{j}{k} \frac{\partial \hat{\psi}(\alpha_s, \beta_t, z')}{\partial z'} = \hat{\psi}'(\alpha_s, \beta_t, z') \tag{37}$$

with

$$\hat{g}^{x'z'}_{p,q} = \frac{\Delta\alpha^2}{4\pi^2} \hat{g}^{x'z'}(\alpha_p, \beta_q) \tag{38}$$

$$\hat{g}^{y'z'}_{p,q} = \frac{\Delta\alpha^2}{4\pi^2} \hat{g}^{y'z'}(\alpha_p, \beta_q) \tag{39}$$

$$\hat{g}^{z'z'}_{p,q} = \delta_{pq} + \sum_{u,v} \hat{g}^{x'z'}_{p-u,q-v} \hat{g}^{x'z'}_{u,v} + \sum_{u,v} \hat{g}^{y'z'}_{p-u,q-v} \hat{g}^{y'z'}_{u,v} \tag{40}$$

where δ_{pq} denotes the Kronecker symbol. Equations (36) and (37) can be written in matrix form

$$\frac{j}{k} \mathbf{L}_l \frac{\partial}{\partial z'} \begin{pmatrix} \vec{\psi} \\ \vec{\psi}' \end{pmatrix} = \mathbf{L}_r \begin{pmatrix} \vec{\psi} \\ \vec{\psi}' \end{pmatrix} \tag{41}$$

$\mathbf{L}_l$ and $\mathbf{L}_r$ are square matrices specified by the left-hand side and the right-hand side of (36) and (37). With a Mth-order truncated approximation, the matrices $\mathbf{L}_l$ and $\mathbf{L}_r$ are $2M_s$-dimensional

ones with $M_s = (2M+1)^2$. The upper vector $\vec{\psi}$ and the lower vector $\vec{\psi}'$ have components $\hat{\psi}(\alpha_s, \beta_t, z')$ and $\hat{\psi}'(\alpha_s, \beta_t, z')$ with $-M \le s, t \le +M$. The elementary solutions of (41) are defined as follows

$$\begin{pmatrix} \vec{\psi}_{mn} \\ \vec{\psi}'_{mn} \end{pmatrix} = \begin{pmatrix} \vec{\phi}_{mn} \\ \vec{\phi}'_{mn} \end{pmatrix} \exp(-jkr_{mn}\, z') \tag{42}$$

with

$$r_{\mathrm{mn}} \mathrm{L}_l \begin{pmatrix} \vec{\phi}_{mn} \\ \vec{\phi}'_{mn} \end{pmatrix} = \mathrm{L}_r \begin{pmatrix} \vec{\phi}_{mn} \\ \vec{\phi}'_{mn} \end{pmatrix} \tag{43}$$

$\vec{\phi}_{mn}$ and $\vec{\phi}'_{mn}$ represent the upper eigenvector and the lower eigenvector associated with the eigenvalue r_{mn}. We write $\phi_{mn}(\alpha_s, \beta_t)$ and $\phi'_{mn}(\alpha_s, \beta_t)$ the components of vectors $\vec{\phi}_{mn}$ and $\vec{\phi}'_{mn}$, respectively. The eigenvalue problem (43) gives $2M_s$ eigensolutions. According to the sampling theorem [7, 17, 18], the elementary wave functions $\hat{\psi}_{mn}(\alpha, \beta, z')$ and $\hat{\psi}'_{mn}(\alpha, \beta, z')$ can be constructed from samples $\phi_{mn}(\alpha_s, \beta_t)$ and $\phi'_{mn}(\alpha_s, \beta_t)$ by the following interpolations

$$\hat{\psi}'_{mn}(\alpha, \beta, z') = \exp(-jkr_{mn}z') \times \sum_{s=-M}^{+M} \sum_{t=-M}^{+M} \phi'_{mn}(\alpha_s, \beta_t) \mathrm{sinc}\left(\frac{\pi}{\Delta\alpha}(\alpha - \alpha_s)\right) \mathrm{sinc}\left(\frac{\pi}{\Delta\alpha}(\beta - \beta_t)\right) \tag{44}$$

$$\hat{\psi}'_{mn}(\alpha, \beta, z') = \exp(-jkr_{mn}z') \times \sum_{s=-M}^{+M} \sum_{t=-M}^{+M} \phi'_{mn}(\alpha_s, \beta_t) \mathrm{sinc}\left(\frac{\pi}{\Delta\alpha}(\alpha - \alpha_s)\right) \mathrm{sinc}\left(\frac{\pi}{\Delta\alpha}(\beta - \beta_t)\right) \tag{45}$$

Function $\hat{\psi}_{mn}(\alpha, \beta, z')$ represents an outgoing wave propagating with no attenuation if $Re(r_{mn}) > 0$ and $\mathrm{Im}(r_{mn}) = 0$. For an evanescent wave, $\mathrm{Im}(r_{mn}) < 0$. It is observed numerically that among the $2M_s$ eigenfunctions (44), M_s of them correspond to outgoing waves ($(m, n) \in D_s$) and as many to incoming waves. The numerically computed eigenvalues and eigenvectors depend on the truncation order M. Depending on whether M is a sufficiently large number, we note numerically that the real eigenvalues r_{mn} are on the interval $[-1;+1]$ and correspond to the cosine of scattering angles with $r_{mn} = \cos\theta_{mn}$ [8]. We can write

$$r_{mn}^2 = \frac{\gamma^2(\alpha_m, \beta_n)}{k^2} = 1 - \left(\frac{\alpha_m}{k}\right)^2 - \left(\frac{\beta_n}{k}\right)^2 = \cos^2(\theta_{mn}) \tag{46}$$

Finally, the Fourier transform of Oz-component is defined as a linear combination of M_s eigensolutions (44) satisfying the outgoing wave condition.

$$\hat{\psi}_d(\alpha, \beta, z') = \sum_{(m,n)\in D_s} A_{mn} \hat{\psi}_{mn}(\alpha, \beta, z') \tag{47}$$

$$\hat{\psi}'_d(\alpha, \beta, z') = \sum_{(m,n)\in D_s} A_{mn} \hat{\psi}'_{mn}(\alpha, \beta, z') \tag{48}$$

Substituting $E_{z'} = 0$ into Equations (28) to (31) and applying the same procedure in the spectral domain, we obtain the Fourier transforms of h-polarised transverse components.

$$\hat{\psi}_{dT}^{(\mathrm{ha})}(\alpha, \beta, z') = \sum_{(m,n)\in D_s} A_{mn}^{(\mathrm{ha})}\, \hat{\psi}_{T,mn}^{(\mathrm{ha})}(\alpha, \beta) \exp(-jkr_{mn}z') \tag{49}$$

with

$$\hat{\psi}_{dT}^{(\mathrm{ha})}(\alpha, \beta, z') = \begin{pmatrix} \hat{E}_{dx'}^{(\mathrm{ha})}(\alpha, \beta) \\ \hat{E}_{dy'}^{(\mathrm{ha})}(\alpha, \beta) \\ Z\hat{H}_{dx'}^{(\mathrm{ha})}(\alpha, \beta) \\ Z\hat{H}_{dy'}^{(\mathrm{ha})}(\alpha, \beta) \end{pmatrix} \text{ and } \hat{\psi}_{T,mn}^{(\mathrm{ha})}(\alpha, \beta) = \begin{pmatrix} \hat{E}_{x',mn}^{(\mathrm{ha})}(\alpha, \beta) \\ \hat{E}_{y',mn}^{(\mathrm{ha})}(\alpha, \beta) \\ Z\hat{H}_{x',mn}^{(\mathrm{ha})}(\alpha, \beta) \\ Z\hat{H}_{y',mn}^{(\mathrm{ha})}(\alpha, \beta) \end{pmatrix} \tag{50}$$

According to the sampling theorem [17, 18], we write

$$\hat{\psi}_{T,mn}^{(\mathrm{ha})}(\alpha, \beta) = \sum_{s=-M}^{+M} \sum_{t=-M}^{+M} \hat{\psi}_{T,mn}^{(\mathrm{ha})}(\alpha_s, \beta_t) \mathrm{sinc}\left(\frac{\pi}{\Delta\alpha}(\alpha - \alpha_s)\right) \mathrm{sinc}\left(\frac{\pi}{\Delta\alpha}(\beta - \beta_t)\right) \tag{51}$$

where

$$\hat{E}_{x',mn}^{(\mathrm{ha})}(\alpha_s, \beta_t) = -k^2 \sum_{p=-M}^{+M} \sum_{q=-M}^{+M} \hat{g}_{s-p,t-q}^{y'z'} \phi'_{mn}(\alpha_p, \beta_q) - k\beta_t \phi_{mn}(\alpha_s, \beta_t) \tag{52}$$

$$\hat{E}_{y',mn}^{(\mathrm{ha})}(\alpha_s, \beta_t) = k^2 \sum_{p=-M}^{+M} \sum_{q=-M}^{+M} \hat{g}_{s-p,t-q}^{x'z'} \phi'_{mn}(\alpha_p, \beta_q) + k\alpha_s \phi_{mn}(\alpha_s, \beta_t) \tag{53}$$

$$Z\hat{H}_{x',mn}^{(\mathrm{ha})}(\alpha_s, \beta_t) = -k^2 \sum_{p=-M}^{+M} \sum_{q=-M}^{+M} \hat{g}_{s-p,t-q}^{x'z'} \phi_{mn}(\alpha_p, \beta_q) - k\alpha_s \phi'_{mn}(\alpha_s, \beta_t) \tag{54}$$

$$Z\hat{H}_{y',mn}^{(\mathrm{ha})}(\alpha_s, \beta_t) = -k^2 \sum_{p=-M}^{+M} \sum_{q=-M}^{+M} \hat{g}_{s-p,t-q}^{y'z'} \phi_{mn}(\alpha_p, \beta_q) - k\beta_t \phi'_{mn}(\alpha_s, \beta_t) \tag{55}$$

Taking $H_{z'} = 0$ and substituting $\vec{E}^{(\mathrm{ha})}$ by $Z\vec{H}^{(\mathrm{va})}$ and $Z\vec{H}^{(\mathrm{ha})}$ by $-\vec{E}^{(\mathrm{va})}$ in (49) to (55), we obtain the v- polarized components of magnetic and electric-fields.

3.3. *Boundary conditions and Scattering amplitudes*

The scattering amplitudes $A_{mn}^{(\mathrm{ha})}$ and $A_{mn}^{(\mathrm{va})}$ are found by solving the boundary conditions. The electric field components $E_{x'}$ and $E_{y'}$ are parallel to surfaces $z' = \mathrm{z}_0$ and appear in the boundary conditions at $z' = 0$, i.e. at $z = a(x, y)$. So, for an incident wave in (a) polarization, we can write

$$E_{dx'}^{(\mathrm{ha})}(x', y', z') + E_{dx'}^{(\mathrm{va})}(x', y', z') = -\left(E_{ix'}^{(\mathrm{a})}(x', y', z') + \rho^{(a)} E_{rs,x'}^{(\mathrm{a})}(x', y', z')\right)$$

$$E^{(\mathrm{ha})}_{dy'}(x', y', z') + E^{(\mathrm{va})}_{dy'}(x', y', z') = -\left(E^{(\mathrm{a})}_{iy'}(x', y', z') + \rho^{(a)} E^{(\mathrm{a})}_{rs,y'}(x', y', z')\right) \tag{56}$$

After a Fourier transform, the point-matching method is applied to (56) at discrete values $(\alpha_s; \beta_t)$. According to Equations (4) to (7), (24), (49) and (56), a $2M_s$-dimensional matrix system is obtained, the inversion of which leads to scattering amplitudes $A^{(\mathrm{ha})}_{mn}$ and $A^{(\mathrm{va})}_{mn}$.

The bi-static scattering coefficients $\sigma^{(\mathrm{ba})}(\theta, \varphi)$ are defined from the scattering amplitudes $\hat{R}^{(\mathrm{ba})}(\alpha, \beta)$ (17). Outside the modulated zone, the Fourier-Rayleigh integrals are valid. So, for a scattered field in (h) polarisation, according to Equations (10), (12), (13), (24) and (49), the following continuity relations on transverse electric components can be written:

At $z_0 > \max(a(x, y))$, $\forall x, y$,

$$E^{(\mathrm{ha})}_{dx'}(x, y, z'_0) = -\frac{1}{4\pi^2}\int_{-\infty}^{+\infty}\int_{-\infty}^{+\infty}\frac{\beta\ \hat{R}^{(\mathrm{ha})}(\alpha, \beta)}{\sqrt{\alpha^2+\beta^2}}\ \exp\left(-j\alpha x - j\beta y - j\gamma\, z_0\right) d\alpha\, d\beta$$

$$E^{(\mathrm{ha})}_{dy'}(x, y, z'_0) = \frac{1}{4\pi^2}\int_{-\infty}^{+\infty}\int_{-\infty}^{+\infty}\frac{\alpha\ \hat{R}^{(\mathrm{ha})}(\alpha, \beta)}{\sqrt{\alpha^2+\beta^2}}\ \exp\left(-j\alpha x - j\beta y - j\gamma\, z_0\right) d\alpha\, d\beta \tag{57}$$

with $z'_0 = z_0 - a(x, y)$. Function $\hat{R}^{(\mathrm{ha})}(\alpha, \beta)$ is obtained by solving the continuity relations (57) in the spectral domain. In final, we find

$$\hat{R}^{(\mathrm{ha})}(\alpha, \beta) = \left(\frac{\alpha}{\sqrt{\alpha^2+\beta^2}}\mathrm{TF}\left[E^{(\mathrm{ha})}_{dy'}(x, y, z'_0)\right] - \frac{\beta}{\sqrt{\alpha^2+\beta^2}}\mathrm{TF}\left[E^{(\mathrm{ha})}_{dx'}(x, y, z'_0)\right]\right)\exp(j\gamma\, z_0) \tag{58}$$

For a scattered field in (v) polarisation, the scattering amplitudes $\hat{R}^{(\mathrm{va})}(\alpha, \beta)$ are derived from the continuity relations of transverse magnetic field components.

4. Scattering by random rough surfaces

4.1. *Generation of the random surface*

First, we consider an isotropic random process $g(x, y)$ with a Gaussian height probability distribution characterized by the root-mean-square height h. The average value of the Gaussian variate $g(x, y)$ is zero. The correlation function used is also Gaussian. l_c is the correlation radius. The realizations are obtained by a Gaussian filter applied to random uncorrelated numbers characterized by a normalized Gaussian distribution [15, 19]. In the second stage, the local function $a(x, y)$ is defined

$$a(x, y) = g(x, y)V(x)V(y) \tag{59}$$

with

$$V(x) = 0 \text{ if } |x| > +\frac{L}{2} \tag{60a}$$

$$V(x) = 1 \text{ if } -\frac{L}{2} + l_t < x < +\frac{L}{2} - l_t \tag{60b}$$

$$V(x) = \frac{x + L/2}{l_t} - \frac{1}{2\pi}\sin\left(\frac{2\pi}{l_t}\left(x + \frac{L}{2}\right)\right) \text{ if } -\frac{L}{2} < x < -\frac{L}{2} + l_t \tag{60c}$$

$$V(x) = \frac{L/2 - x}{l_t} - \frac{1}{2\pi}\sin\left(\frac{2\pi}{l_t}\left(\frac{L}{2} - x\right)\right) \text{ if } \frac{L}{2} - l_t < x < \frac{L}{2} \tag{60d}$$

$V(x)$ is a step function having continuous first and second derivatives and equal to zero outside the interval $[-L/2; +L/2]$. The rough surface $z = a(x, y)$ has a finite modulation area $L \times L$ with transition zones of width l_t [7, 15]. It is worth noting that the profile $g(x, y)$ and the distribution of height are unchanged when $-\frac{L}{2} + l_t < x, y < +\frac{L}{2} - l_t$.

4.2. *Coherent intensity and incoherent intensity*

The averaged bi-static coefficient is defined as follows [7]

$$\begin{aligned}\langle \sigma^{(\mathrm{ba})}(\theta, \varphi)\rangle &= I_c^{(\mathrm{ba})}(\theta, \varphi) + I_f^{(\mathrm{ba})}(\theta, \varphi) \\ &= \frac{1}{\lambda^2 \mathrm{L}^2}\frac{\cos^2\theta}{\cos\theta_i}\left\langle \left|\hat{R}^{(\mathrm{ba})}(k\sin\theta\cos\varphi; k\sin\theta\sin\varphi)\cos\theta\right|^2\right\rangle\end{aligned} \tag{61}$$

where the angular bracket $\langle\rangle$ stand for ensemble averaging. $I_c^{(\mathrm{ba})}(\theta, \varphi)$ is the coherent intensity and $I_f^{(\mathrm{ba})}(\theta, \varphi)$, the incoherent intensity.

$$I_c^{(\mathrm{ba})}(\theta, \varphi) = \frac{1}{\lambda^2 \mathrm{L}^2}\frac{\cos^2\theta}{\cos\theta_i}\left|\left\langle \hat{R}^{(\mathrm{ba})}(k\sin\theta\cos\varphi; k\sin\theta\sin\varphi)\right\rangle\right|^2 \tag{62}$$

Some authors prefer to use the normalized incoherent radar cross-section ($4\pi\cos\theta_i I_f^{(\mathrm{ba})}(\theta, \varphi)$). The Monte Carlo technique is applied to estimate the averaged bi-static coefficient and the incoherent intensity from the results over N_R different realizations [7].

5. Results

5.1. *Truncation order and size of matrices*

In the spectral domain, the Mth-order truncation removes the highest spatial frequencies of the field components. As a consequence, the part of the electromagnetic field consisting of higher order evanescent eigen waves is also removed. So, integration variables α and β vary within interval $[-\alpha_{\max}; +\alpha_{\max}]$ with

$$\alpha_{\max} = \alpha_M = M\Delta\alpha \tag{63}$$

The proportion of evanescent waves is larger when $\alpha_{\max}$ increases, so that the coupling phenomena are better described. We can note that in the convolution products of Equations (36) and (52)–(54),

integration variables α and β for the Fourier transforms of metric tensor elements vary within the interval $[-2\alpha_{\max}; +2\alpha_{\max}]$.

The C method requires solving a $2M_s$-dimensional eigenvalue system and inverting a $2M_s$-dimensional matrix that leads to the scattering amplitudes. The C method has been implemented in Matlab language on several Xeon-Pentium-3.4 GHz- bi-processor PC with 4 GB RAM.

5.2. *Results for a single surface*

We consider a single surface with an area of $L^2 = 64\lambda^2$ and illuminated under incidence angles $\theta_i = 30^\circ$ and $\varphi_i = 0^\circ$. The Gaussian random surface has a correlation length $l_c = \lambda$. If the method is numerically stable, the accuracy on the power balance and the results increase with increasing the truncation order M. To illustrate this idea, two measures of error are defined as follows

$$\Delta P^{(a)} = \left|1 - P_{si}^{(a)} / P_s^{(a)}\right| \tag{64}$$

$$\Delta F^{(\mathrm{ba})} = \frac{\int_{-\pi/2}^{+\pi/2} \left| F_{\mathrm{ref}}^{(\mathrm{ba})}(\theta, \varphi) - F^{(\mathrm{ba})}(\theta, \varphi) \right| d\theta}{\int_{-\pi/2}^{+\pi/2} F_{\mathrm{ref}}^{(\mathrm{ba})}(\theta, \varphi)\, d\theta} \tag{65}$$

$\Delta P^{(a)}$ defines the error on the power balance for the incident polarization (a) and $\Delta F^{(\mathrm{ba})}$, a relative error between the energetic magnitude under study $F^{(\mathrm{ba})}(\theta)$ and the reference energetic magnitude $F_{\mathrm{ref}}^{(\mathrm{ba})}(\theta)$ obtained from experiment data or another exact method. $F^{(\mathrm{ba})}$ represents either $\sigma^{(\mathrm{ba})}$ or $\langle \sigma^{(\mathrm{ba})} \rangle$ obtained in the plane of incidence.

Table 1 lists the errors $\Delta P^{(a)}$ for different pairs $(h; M)$ in both polarizations and shows that for a given rms height, the errors decrease with increasing the truncation order. We can also point out that the more h increases, the slower the power balance converges (The surfaces under consideration are obtained by a proportional transformation). This means that as the rms height increases, more and more evanescent waves must be taken into consideration to describe the scattering phenomenon. If we consider the h-polarized plane wave incidence and a truncation order M of 12, the maximum value that the rms height can reach is about 0.45λ in order to satisfy the power balance to within 1%. With $M = 24$, the maximum value is about 0.75λ. If we consider the v-polarized plane wave incidence, the corresponding values are about 0.35λ and 0.8λ, respectively. Table 2 lists the higher spatial frequency, the number of unknowns and the CPU time for several truncation orders. With $M = 12$ and $M = 24$, the method gives 1250 and 4802 unknowns amplitudes, respectively. As shown in Table 2, the computation time varies approximately as M_s^3.

It's important to show that an electromagnetic model checks the power balance. Nevertheless, the power balance criterion is not sufficient to ensure the validity of any numerical method. So, it's important to study the convergence of the C-method results with respect to the truncation order [5] and to verify the theory by comparison with other exact methods and experimental data. Figure 1 shows the normalised bi-static scattering coefficient $\sigma^{(\mathrm{vh})}$ in the plane of incidence for various truncation order values. The rms height is $h = 0.4$ wavelength. The convergence on results is ensured for $M \geq 16$. Relative error $\Delta\sigma^{(\mathrm{vh})}(\theta)$ between $\sigma^{(\mathrm{vh})}(\theta, M = 16)$ and $\sigma_{\mathrm{ref}}^{(\mathrm{vh})}(\theta, M = 28)$ is equal to 5%. With $M = 16$, the error on power balance is weak, the accuracy on far-field results is good and the computation time is reasonable (12 minutes). Figure 2 shows the normalized

Table 1. Error ΔP on the power balance versus truncation order and rms height. The surfaces under consideration are obtained by a proportional transformation. Rough-surface parameters: $l_c = \lambda$, $l_t = \lambda/2$, $L = 8\lambda$; incident angles: $\theta_i = 30^\circ$ and $\varphi_i = 0^\circ$; Spectral resolution: $\Delta\alpha = \mathrm{k}\,/\,8$.

M / h	Error	0.2 λ	0.4 λ	0.6 λ	0.8 λ	1.0 λ
12	$\Delta P^{(h)}$	1.0×10^{-4}	5.0×10^{-3}	0.14	2.2	6310
	$\Delta P^{(v)}$	4.0×10^{-4}	1.6×10^{-2}	4.0×10^{-2}	2.6	1585
16	$\Delta P^{(h)}$	1.3×10^{-4}	1.3×10^{-3}	6.3×10^{-3}	0.05	63
	$\Delta P^{(v)}$	4.0×10^{-4}	2.5×10^{-3}	3.2×10^{-3}	0.1	40
20	$\Delta P^{(h)}$	7.9×10^{-6}	3.2×10^{-4}	3.2×10^{-3}	2.5×10^{-2}	4.0
	$\Delta P^{(v)}$	3.2×10^{-6}	4.0×10^{-4}	4.0×10^{-3}	1.3×10^{-2}	1.6
24	$\Delta P^{(h)}$	1.6×10^{-6}	1.0×10^{-4}	1.9×10^{-3}	1.6×10^{-2}	0.32
	$\Delta P^{(v)}$	1.6×10^{-7}	5.0×10^{-5}	7.9×10^{-4}	1.0×10^{-2}	0.25
28	$\Delta P^{(h)}$	1.0×10^{-7}	2.0×10^{-5}	4.0×10^{-4}	6.3×10^{-3}	1×10^{-2}
	$\Delta P^{(v)}$	7.9×10^{-8}	2.0×10^{-5}	2.0×10^{-4}	4×10^{-3}	2×10^{-2}

bi-static scattering coefficient $\sigma^{(vh)}$ with a rms height $h = 0.8$ wavelength. The convergence is ensured if the truncation order is larger than 24. Relative error $\Delta\sigma^{(vh)}(\theta)$ between $\sigma^{(vh)}(\theta, M = 24)$ and $\sigma^{(vh)}_{ref}(\theta, M = 28)$ is equal to 9%. With $M = 24$, the CPU time becomes important (135 minutes).

In the next section, we present some results obtained by the C method for perfectly conducting surfaces illuminated by an incident plane wave and we check their validity against the scattering patterns given by methods based on solutions of surface integral equations [20, 21] and given by experiments [22].

5.3. *Comparison with exact numerical simulations and experimental data*

We consider random rough surfaces with an area of $L^2 = 64\lambda^2$ illuminated under incidence angles $\theta_i = 10^\circ$ and $\varphi_i = 0^\circ$. The rms height is $h = 0.2$ wavelength with a correlation radius $l_c = 0.6$ wavelength. Figure 3 shows the averaged bi-static coefficient in the plane of incidence with a (h)-polarized incident plane wave. The co-polarized component $< \sigma^{(hh)} >$ and the cross-polarized component $\langle \sigma^{(vh)} \rangle$ are performed over $N_R = 780$ realizations. In Figure 3, the Monte-Carlo simulation results given by the SMFSIA/CAG method (Sparse-Matrix Flat-Surface Iterative Approach with CAnonical Grid) are also plotted [20]. The authors in [20] have used surfaces with an area of 256 square wavelengths illuminated by a tapered wave [23]. The ensemble averaging is performed over 280 realizations that are different from 780 realizations used for our simulation. The comparison is satisfactory. Relative error $\Delta\sigma^{(hh)}$ is equal to 10% and $\Delta\sigma^{(vh)}$

Table 2. System size, higher spatial frequency and CPU time versus truncation order. The parameters are those of Table 1.

M	$2M_s = 2\,(2M + 1)^2$	$2\alpha_{max}$	Speed
12	1250	$3k$	130 sec
16	2178	$4k$	12 min
20	3362	$5k$	45 min
24	4802	$6k$	2 h 15 min
28	6498	$7k$	5 h 40 min

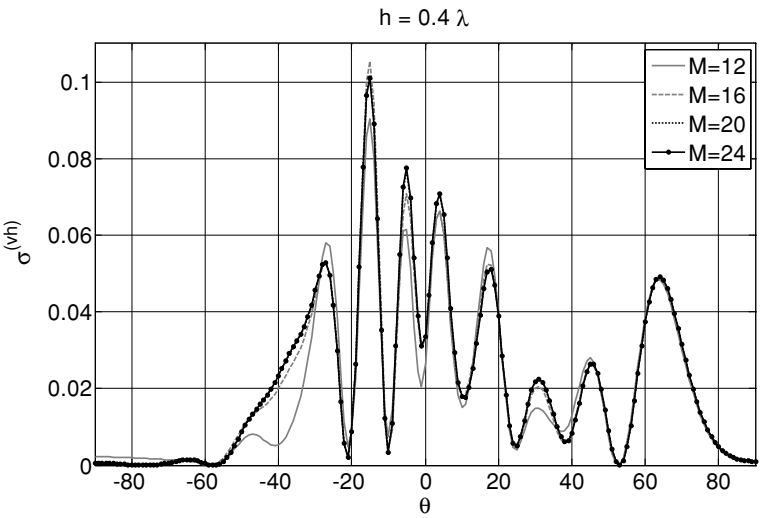

Figure 1. Bi-static scattering coefficient $\sigma^{(\mathrm{hv})}$ in the plane of incidence for one realization with $h = 0.4\lambda$. The parameters are those of Table 1.

is equal to 7% (The reference scattered pattern is given by the SMFSIA/CAG method). The cell areas, the illumination laws and the realizations used for the two theories are different and explain the differences observed on results. For our Monte-Carlo simulation results, the truncation order is fixed at 18. Figures 4 and 5 give the normalized histograms of errors $\Delta P^{(\mathrm{h})}$ and $\Delta P^{(\mathrm{v})}$, respectively. These histograms show that the error is smaller than 10^{-3} for eight realizations in 10, and the error is smaller than 1% for all the realizations.

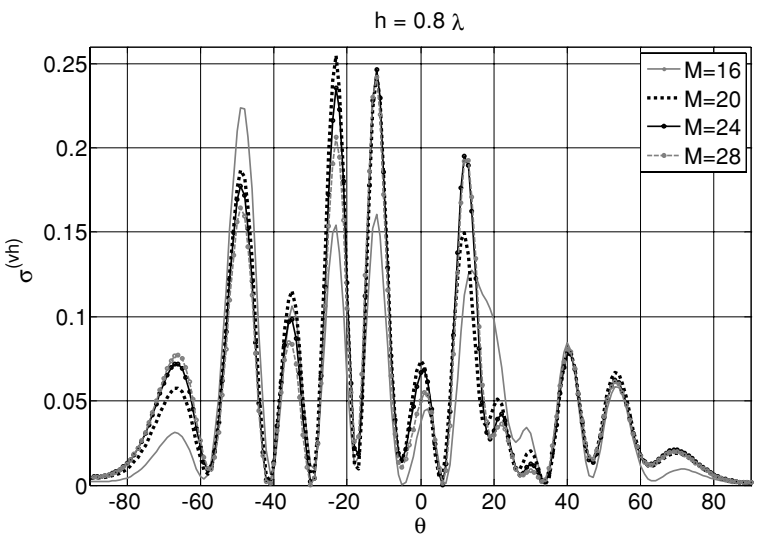

Figure 2. Bi-static scattering coefficient $\sigma^{(\mathrm{hv})}$ in the plane of incidence for one realization with $h = 0.8\lambda$. The parameters are those of Table 1.The surfaces under consideration in Figures 1 and 2 are obtained by a proportional transformation.

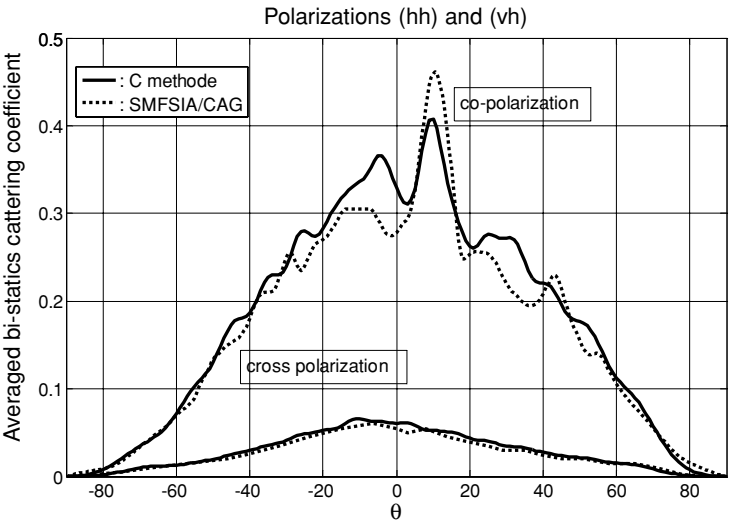

Figure 3. Comparison between the SMFSIA/CAG method and the C method: Averaged bi-static scattering coefficient in the plane of incidence, (h) incidence. Rough-surface parameters $h = 0.2\lambda, l_c = 0.6\lambda, l_t = l_c/2$, $L = 8\lambda$; incident angles $\theta_i = 10^\circ$ and $\varphi_i = 0^\circ$; Spectral resolution $\Delta\alpha = k/8$. Truncation order $M = 18$; Number of realizations $N_R = 780$. Results of the SMFSIA/CAG method are taken in [20].

In Figure 6, the averaged bi-static coefficient is plotted in the plane incidence for the cross-polarized incoherent intensities ($4\pi \cos\theta_i I_f^{(\mathrm{vh})}$ and $4\pi \cos\theta_i I_f^{(\mathrm{hv})}$). We consider random rough surfaces with an area of $L^2 = 64\lambda^2$ illuminated under incidence $\theta_i = 40^\circ$ and $\varphi_i = 0^\circ$. The rms height is $h = 0.5$ wavelength with a correlation radius $l_c = 1.41$ wavelength. Each elementary cell dimensions are about 32 square correlation lengths. The averaged bi-static coefficients are performed over $N_R = 300$ realizations. With $M = 18$, the error on the power balance is smaller than 1% for all the realizations. In Figure 6, the Monte-Carlo simulation results given by the FB-NSA method (Forward-Backward/Novel Spectral Acceleration method) are also plotted [21]. The authors in [21] have used surfaces with an area of 128×32 square wavelengths illuminated by a tapered wave. The ensemble averaging is performed over 150 realizations. Although the elementary cell area is reduced to $32l_c^2$, comparison is satisfactory.

Figure 7 shows the averaged bi-static coefficients in the plane of incidence for Monte Carlo simulations and millimeter-wave experiments under v-polarized incident waves [22]. The rms height is $h = 1$ wavelength with a correlation radius $l_c = 1.41$ wavelength. For our simulations, the incident plane wave is characterized by the zenith angle $\theta_i = 20^\circ$ and the azimuth angle $\varphi_i = 0^\circ$. Elementary cells present an area of 64 square wavelengths. We generate 300 elementary surfaces and for each realization, we use a truncation order that leads to an error on the power balance smaller than 5%. With $M = 21$, the power balance criterion is verified on 236 realizations. Among the remaining 64 realizations, the truncation order is fixed at 24 and the criterion is verified on 48 realizations. Among the remaining 16 realizations, the truncation order is fixed at 28 and the criterion is only verified for 13 realizations. The curves in Figure 8 are performed over these 297 realizations. Although the elementary cell area is reduced to $32l_c^2$, the comparison with experimental data is satisfactory. Relative error $\Delta\sigma^{(\mathrm{vv})}$ is equal to 13% and $\Delta\sigma^{(\mathrm{hv})}$ is equal to 12% (The reference scattered patterns are given by experiment data). The backscattering peaks coincide well enough.

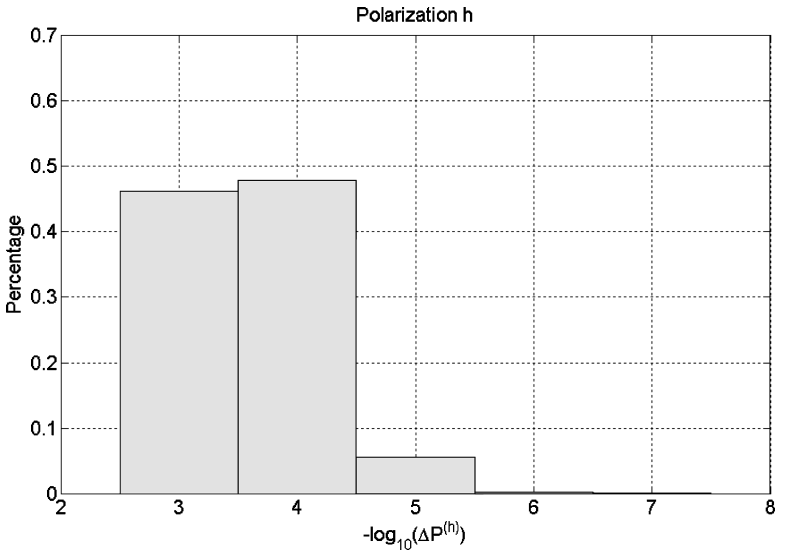

Figure 4. Histogram of errors $\Delta P^{(\mathrm{h})}$. The parameters are those of Figure 3.

In this section, we have presented some results obtained by the C method and we check their validity against the scattering patterns given by numerical methods based on solutions of surface integral equations and by experimental data. For a monochromatic plane wave incidence, edge effects can appear. Nevertheless, we use the step function defined by Equation (60) and the comparisons are conclusive in both fundamental polarizations for a relatively wide range of incidence angles ($\theta_i \leq 40^\circ$). The surfaces under study present relatively large slopes ($\sqrt{2}h/l_c \leq 1$ and $0.5 \leq l_c \leq \sqrt{2}$) for which the predictions of the standard analytic methods (Kirchhoff

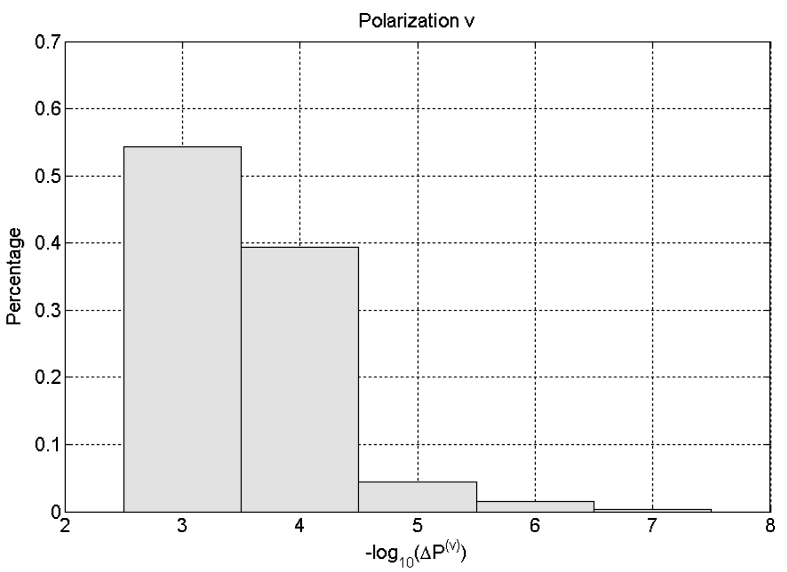

Figure 5. Histogram of errors $\Delta P^{(\mathrm{v})}$. The parameters are those of Figure 3.

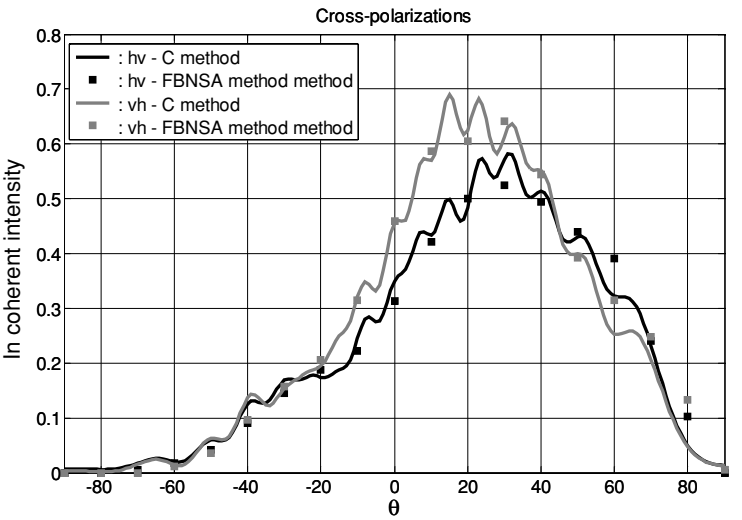

Figure 6. Comparison between the FBNSA method and the C method: Normalized incoherent radar cross-section in the plane of incidence for both cross-polarizations. Rough-surface parameters $h = 0.5\lambda, l_c = \sqrt{2}\lambda$, $l_t = \lambda/2$, $L = 8\lambda$; incident angles $\theta_i = 40^\circ$ and $\varphi_i = 0^\circ$; Spectral resolution $\Delta\alpha = k/8$. Truncation order $M = 18$; Number of realizations $N_R = 300$. Results of the FBNSA method are taken in [21].

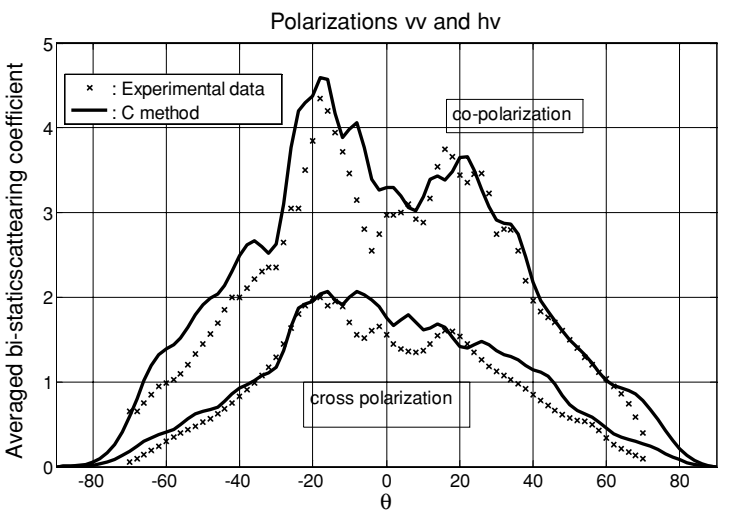

Figure 7. Monte-Carlo simulation comparison of the C method and the experimental data: Averaged bi-static scattering coefficient in the plane of incidence, (v) incidence. Rough-surface parameters $h = \lambda$, $l_c = \sqrt{2}\lambda, l_t = \lambda/2, L = 8\lambda$; incident angles $\theta_i = 20^\circ$ and $\varphi_i = 0^\circ$; Spectral resolution $\Delta\alpha = k/8$. Truncation order $M = 21$, $M = 24$ or $M = 28$; Number of realisations $N_R = 297$. Experimental data are taken in [22].

approach, small perturbation method, small slope approximation) are inaccurate [24–25]. The Monte-Carlo simulations based on the C method have been successful in predicting backscattering enhancement.

5.4. *The C-method and the boundary integral methods*

The boundary integral method can be used for analysing the scattering problem by rough surfaces. In this case, the electric or magnetic field integral equation is converted into matrix equations using the method of moments in the spatial domain [3]. If the surface sampling step is $\lambda/7$, the sample number of the surface of length $L = 8\lambda$ is 3136 and the size of matrices to be treated is 6272. This size is given by the C method with a truncation order equal to $M = 28$. For this example, the system sizes are similar for both methods. But, we cannot conclude in terms of trade-off 'accuracy versus computation time'. This conclusion should be based on a serious numerical investigation that requires implementing both methods on the same workstation with the same programming language and for a large number of configurations, comparing the computation times with the same accuracy in results. But, the C-method is based on the definition of the eigensolutions of the scattering problem. As a result, the curvilinear coordinate method is an accurate one. We think that it's the main advantage by using the C-method.

Nevertheless, what should be kept in mind is that the dominant computational cost for the C method is the eigenvalue problem solution which is of the order of M_s^3 (For $M = 16$, the eigenvalue problem solution requires 11 over 12 minutes total CPU time). The computational costs for the boundary integral equation are the matrix fill time which is of the order of M_s^2 and the linear system solution which ranges from $O(M_s^2)$ for iterative algorithm applied to well conditioned operators or to $O(M_s^3)$ for direct matrix factorization methods [3]. Several classes of methods have been proposed to reduce the CPU time. These methods enable us to obtain the field scattered from surface of very large size [20, 21, 26–32]. Owing to computational costs, the C method in the present form doesn not enable us to analyse the surfaces of very large sizes and the surfaces with large transverse correlation length. This is a weak point of the C method. Moreover, numerical simulations of rough surface scattering at near-grazing incidence requires very large surfaces [33, 34]. The C-method in the present form isn't suitable to analyse this particular scattering problem.

In the next step of our work, we will propose to reduce the computational time by the implementation of the short-coupling-range approximation [26]. This approach has been successfully implemented in the case of 1-D rough surfaces [35]. It amounts to represent a scattering surface by several elementary surfaces of shorter size and leads to analyse the electromagnetic couplings between the elementary cells.

6. Conclusion

In this paper, for the first time, the curvilinear coordinate method has been applied for analysing 2-D perfectly conducting random rough surfaces. The method has been numerically investigated in the far-field zone. The numerical stability of bi-static coefficient is ensured and the accuracy on power balance increases with the truncation order. The Monte Carlo technique has been applied for estimating the bi-static scattering coefficient and the incoherent intensity from the results over several realisations. The comparisons with published numerical and experimental data are satisfactory in both co-polarised and cross-polarised components and allow the validity of our computer code to be checked. Extension of the C method to dielectric rough 2-D surfaces is currently under investigation.

Acknowledgment

The authors thank the 'Programme National de Télédétection Spatiale' that has supported the research of this paper.

References

[1] J.A. Ogilvy, *Theory of Wave Scattering from Random Rough Surfaces*, Hilger, Bristol, 1991.
[2] L. Tsang, J.A. Kong, K.H. Ding, and C.O. Ao, *Scattering of Electromagnetic Waves – Numerical Simulations*, Wiley-Interscience, New York, 2001.
[3] K.F. Warnick and W.C. Chew, *Numerical simulation methods for rough surface scattering*, Waves Random Media 11 (2001), R1–R30.
[4] M. Saillard and A. Sentennac, *Rigorous solutions for electromagnetic scattering from rough surfaces*. Waves Random Media 11 (2001), pp. R103–R137.
[5] R. Dusséaux and R. de Oliveira, *Scattering of a plane wave by 1-dimensional rough surface – Study in a nonorthogonal coordinate system*, PIER 34 (2001), pp. 63–88.
[6] R. Dusséaux and C. Baudier, *Scattering of a plane wave by 1-dimensional dielectric rough surfaces – study of the field in a nonorthogonal coordinate system*, PIER 37 (2003), pp. 289–317.
[7] C. Baudier, R. Dusséaux, K.S. Edee, and G. Granet, *Scattering of a plane wave by one-dimensional dielectric random surfaces – study with the curvilinear coordinate method*, Waves Random Media 14 (2004), pp. 61–74.
[8] J. Chandezon, D. Maystre, and G. Raoult, *A new theoretical method for diffraction gratings and its numerical application*, J. Opt (Paris) 11 (1980), pp. 235–241.
[9] L. Li and J. Chandezon, *Improvement of the coordinate transformation method for surface-relief gratings with sharp edges*, J. Opt. Soc. Am. A 13 (1995), pp. 2247–2255.
[10] G. Granet, *Diffraction par des surfaces bi-périodiques: résolution en coordonnées non orthogonales*, Pure Appl. Opt. 4 (1995), pp. 777–793.
[11] P.M. Van Den Berg, and J.T. Fokkema, *The Rayleigh hypothesis in the theory of diffraction by a perturbation in a plane surface*, Radio Sci. 15 (1980), pp. 723–732.
[12] A. Voronovich, *Small-slope approximation for electromagnetic wave scattering at a rough interface of two dielectric half-spaces*, Waves Random Media 4 (1994), pp. 337–367.
[13] M. Born and E. Wolf, *Principles of Optics – Electromagnetic Theory of Propagation Interference and Diffraction of Light*, Appendix III, Pergamon, Oxford, 1980.
[14] C. Baudier and R. Dusséaux, *Scattering of an $E_{//}$- polarized plane wave by one-dimensional rough surfaces: numerical applicability domain of a Rayleigh method in the far-field zone*, PIER 34 (2001), pp. 1–27.
[15] D. Maystre, *Electromagnetic scattering from perfectly conducting rough surfaces in the resonance region*, IEEE Trans. Antennas Propagat. 31 (1983), pp. 885–895.
[16] J.A. Stratton, *Electromagnetic Theory*, McGraw-Hill, New York, 1941.
[17] D. Middleton, *Introduction to Statistical Communication Theory*, McGraw-Hill, New York, 1960.
[18] C.E. Shannon, *Mathematical theory of communication*, Bell System Tech. J. 27 (1948), pp. 379–423.
[19] A.K. Fung and M.F. Chen, *Numerical simulation of scattering from simple and composite surface*, J. Opt. Soc. Am. A. 2 (1985), pp. 2274–2283.
[20] K. Pak, L. Tsang, C.H. Chan, and J.T. Johnson, *Backscattering enhancement of electromagnetic waves from two-dimensional perfectly conducting random rough surfaces based on Monte-Carlo simulations.* J. Opt. Soc. Am. A 12 (1995), pp. 2491–2499.
[21] D. Torrungrueng and J.T. Johnson, *Numerical studies of backscattering enhancement of electromagnetic waves from two-dimensional random rough surfaces with the forward-backward/novel spectral acceleration method*. J. Opt. Soc. Am. A. 18 (2001), pp. 2518–2526.
[22] J.T. Johnson, L. Tsang, R.T. Shin, K. Pak, C.H. Chan, A. Ishimaru, and K. Yasuo, *Backscattering enhancement of electromagnetic waves from two-dimensional perfectly conducting random rough surfacers: A comparison of Monte-Carlo simulations with experimental data*, IEEE Trans Antennas Propagat. 44 (1996), pp. 748–756.
[23] E.I. Thorsos, *The validity of the Kirchhoff approximation for rough surface scattering using a Gaussian roughness spectrum*, J. Acoust. Soc. Am. A 82 (1988), pp. 78–92.
[24] T.M. Elfouhaily and C.A. Guérin, *A critical survey of approximate scattering wave theories from random rough surfaces*. Waves Random Media 14 (2004), R1–10.
[25] C.A. Guérin, G. Soriano, and T.M. Elfouhaily, *Weighted curvature approximation: numerical tests for 2D dielectric surfaces*, Waves Random Media 14 (2004), pp. 349–363.

[26] D. Maystre and J.P. Rossi, *Implementation of a rigorous vector theory of speckle for two-dimensional microrough surfaces*, J. Opt. Soc. Am. A 3 (1986), pp. 1276–1282.
[27] M. Saillard and D. Maystre, *Scattering from random rough surfaces: a beam simulation method*, J. Opt (Paris) 19 (1988), pp. 173–176.
[28] G. Soriano and M. Saillard, *Scattering of electromagnetic waves from two-dimensional rough surfaces with an impedance approximation*, J. Opt. Soc. Am. A 18 (2001), pp. 124–133.
[29] R.L. Wagner, J. Song, and W.C. Chew, *Monte Carlo simulations of electromagnetic scattering from two-dimensional random rough surfaces.* IEEE Trans. Antennas Propagat 45 (1997), pp. 235–245.
[30] K. Pak, L. Tsang, and J.T. Johnson, *Numerical simulations and backscattering enhancement of electromagnetic waves from two-dimensional dielectric random rough surfaces with the sparse-matrix canonical grid method.* J. Opt. Soc. Am. A 18 (1997), pp. 1515–1529.
[31] L. Tsang, D. Chen, and P. Xu, *Wave scattering with the UV multilevel partitioning method: 1. Two-dimensional problem of perfect electric conductor surface scattering*, Radio Sci. 39 (2004), pp. 1–13.
[32] L. Tsang, Q. Li, D. Chen, P. Xu, and V. Jandhyala, *Wave scattering with the UV multilevel partitioning method: 2. Three-dimensional problem of nonpenetrable surface scattering*, Radio Sci. 39 (2004), pp. 1–11.
[33] H.D. Ngo and C.L. Rino., *Application of beam simulation to scattering at low grazing angles – 1 Methodology and validation*, Radio Sci. RS00823 (1994), pp. 1365–1379.
[34] H.D. Ngo and C.L. Rino, *Application of beam simulation to scattering at low grazing angles – 2 oceanlike surfaces*, Radio Sci. RS01924 (1994), pp. 1381–1391.
[35] K. Aït Braham and R. Dusséaux, *Analysis of the Scattering from Rough Surfaces with the C Method and the Short-Coupling Range Approximation. Applied Computational Electromagnetics Society Conference (ACES)*.Verona, Italy, March 19–24, 2007, pp. 1880–1886.